Subband structure and scattering mechanisms of a surface two-dimensional electron gas in heavily-doped InAs

V. F. Radantsev, T. I. Deryabina, L. P. Zverev, G. I. Kulaev, and S. S. Khomutova

A. M. Gorkiĭ Ural State University

(Submitted 19 February 1986)
Zh. Eksp. Teor. Fiz. **91**, 1016–1029 (September 1986)

We have investigated both theoretically and experimentally the parameters of the quasi-two-dimensional electron gas present in accumulation layers of n-InAs ($n = 2\times 10^{16}$ to 2×10^{18} cm^{-3}). The $2D$ subband occupation parameters, binding energies and cyclotron masses are determined by analyzing magneto-oscillations in the capacitance, and are found to be in good agreement with the results of quasiclassical calculations. The theory predicts that the $2D$ subband parameters are close for the broad category of semiconductors and semimetals whose energy dispersion is of the Kane form; this closeness is confirmed by the coincidence of experimental data for InAs and $Hg_{1-x}Cd_xTe$ ($x<0.2$), which are the extreme cases of this class of materials. Analysis of the field dependence of the magneto-oscillation amplitude points to the dominance of scattering by ionized donors and surface roughness in the samples under investigation. Because of the effects of nonparabolicity, intersubband screening and intersubband scattering, the contribution of less-populated excited subbands to the total conductivity can frequently exceed the ground-state subband contribution.

1. INTRODUCTION

Two-dimensional ($2D$) electrons in accumulation layers of InAs were studied earlier in Refs. 1, 2. However, the tunnelling-spectroscopy technique used in these papers did not allow controllable variation of the surface carrier density. On the other hand, use of conventional methods based on the field effect for studying accumulation layers are limited to the case of lightly-doped materials (inversion layers of InAs were studied recently using this method in Ref. 3). Whereas both the subband populations and cyclotron masses have been measured for epitaxial layers of InAs with $n\approx 2\times 10^{15}$ cm^{-3} (we should mention in this connection the contradictory data in Refs. 4 and 5), for more heavily-doped samples there is no data available on effective masses. Meanwhile, Ref. 6 shows theoretically how knowledge of these parameters can be used to determine the energy structure of the $2D$ subbands for narrow-gap materials in the presence of a nonparabolic conduction band. As for relaxation times, the available data on inversion layers[3] is based on measurements of the total conductivity, and gives no information on scattering processes within the various subbands. In accumulation layers, because of shunting of the surface conductivity by the volume, galvanometric methods cannot be used to determine the effective channel mobility with any precision even at $n\approx 10^{16}$ cm^{-3}.

In the present paper the method of capacitance spectroscopy in a magnetic field[6,7] is used to study the effects of surface quantization in n-InAs ($n\sim 2\times 10^{16}$–2×10^{18} cm^{-3}). Use of this technique avoids a major difficulty with accumulation layers—coupling of the surface layer and volume electronic subsystems—since it ensures that the capacitance is measured under equilibrium conditions. In addition to determining the two-dimensional subband parameters in InAs accumulation layers, this study is of interest in another respect. In a previous study of accumulation and inversion layers in narrow-gap and semimetallic $Hg_{1-x}Cd_xTe$[6] using the capacitive method, we observed a series of anomalies (disruption of the periodicity of the capacitance magnetic oscillations, weak dependence of the subband parameters on composition, and the presence of localized surface states of resonance type) in comparison with wider-gap semiconductors, whose interpretation remains in general ambiguous. In order to clarify whether or not some of these peculiarities are connected with the multiband nature of the two-dimensional electronic spectrum, or whether the smallness of the energy interval $E_g = E(\Gamma_6) - E(\Gamma_8)$ in $Hg_{1-x}Cd_xTe$ plays an important role, it is of interest to study materials with larger E_g, but which also have some populated $2D$ subbands. In this respect, InAs, which has the largest forbidden gap E_g of the narrow-gap semiconductor series, is in our opinion the most appropriate system to study.

Finally, for InAs—at least for InAs with $n_b < 2\times 10^{16}$ cm^{-3}, and with respect to occupation parameters with $n_b \sim 10^{17}$ cm^{-3} also—there is the possibility of correlating the capacitance spectroscopy data with the results of galvanomagnetic[4] and magneto-optic[8] investigations. In the case of $Hg_{1-x}Cd_xTe$ such a correlation could not be made due to the absence of data obtained by other methods (subband occupation numbers for accumulation layers in weakly-doped $Hg_{1-x}Cd_xTe$ with $n_b \sim 10^{15}$ cm^{-3} were recently determined from magneto-oscillations in the field-dependent mobility[9]).

2. SAMPLE CHARACTERISTICS

We must make one remark in connection with the parameters of the original materials which are presented in the table. Whereas the bulk concentrations (here and henceforth we will denote bulk parameters by the subscript b) determined by the Hall and Shubnikov–de Haas effects coincide within the limits of experimental error, the relaxation

 0038-5646/86/090598-09$04.00 © 1987 American Institute of Physics

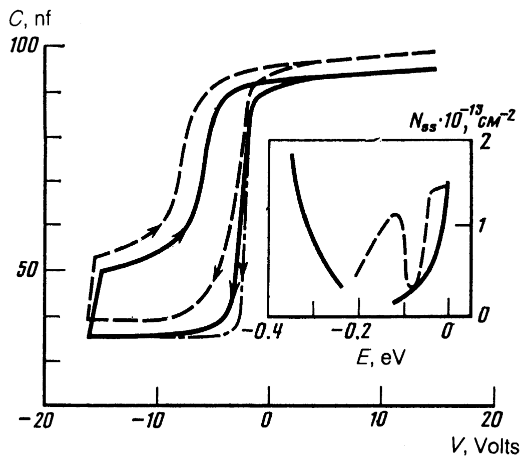

FIG. 1. C-V characteristics and surface-state density (in inset) of a MOS structure based on sample 1 for various values of temperature: the continuous curve is for $T = 4.2$ K, the dashed for 77 K and the dotted-dashed curve is for 4.2 K (theory).

times determined from the Hall mobility μ_{Hb} exceed significantly their values obtained from the Dingle temperature T_{Db}; this difference is most significant for lightly-doped samples. Such behavior is apparently due to fluctuations in n_b.

The original films, after mechanical preparation, ultrasonic cleaning and etching, were anodized in an electrolyte of 5% H_3PO_4 + 45% glycerine + 50% isopropyl alcohol at a current density of 1 mA/cm^2. On each film 5–10 MOS capacitors were fabricated, with areas $\sim 10^{-3}$ cm^2, whose capacitances were measured in the frequency range $f = 3\times 10^4$ to $f = 3\times 10^5$ Hz. The modulation depth of the surface band-bending in the accumulation region when the test signal was applied was less than 100 μV.

The capacitance-voltage characteristics (CVC) of the structures so obtained (shown in Fig. 1 for sample 1) were of high-frequency type in the temperature range under investigation (4 K to 77 K), and were independent of frequency over the entire range of voltage V applied at the field electrode. The values of the concentration n_b obtained from the plateau values of the capacitance in the inversion region were close to those given in the table for all the samples. The flat-band charge on the lower CVC branch was less than $\pm 1.5\times 10^{12}$ cm^{-2} for all samples; the hysteresis width near flat-band is 3–5 V, and grows somewhat as T is increased. In Fig. 1, we also give theoretical CVC calculated for the classical space-charge region (SCR) in the two-band Kane approximation,[10] and in the inset the density of surface states N_{ss} determined by the Terman method. Similar values of N_{ss} for energies near the bottom of the conduction band (0.3 to 1×10^{13} cm^{-2}) were also obtained for more heavily-doped samples. We note that the values given for N_{ss} are apparently overestimated, since certain results which will be presented below suggest that significant fluctuations in the surface potential are present for the structures under investigation.

3. RESULTS OF MEASUREMENTS

Figure 2 shows the magneto-oscillations in the capacitance for fixed V, and the positions of the oscillation maxima in H-V coordinates for sample 2. We detected oscillations in samples 1 and 2 which correspond to the filling of three, and in sample 3 two, size-quantized subbands. In contrast to structures based on $Hg_{1-x}Cd_xTe$[6] investigated earlier, no phase discontinuities in the oscillations were observed for any of the subbands. To a certain extent, this result casts some doubt on the correctness of the hypothesis which was advanced in Ref. 6 to explain the nature of these phase oscillations, i.e., that they are related to simultaneous filling of several subbands in narrow-gap materials. If this assumption were correct, one would expect qualitatively similar behavior of the oscillations for InAs and $Hg_{1-x}Cd_xTe$, since the subband occupation and dispersion-law parameters, as we will show below, are similar in these materials. The disagreement in results for InAs and $Hg_{1-x}Cd_xTe$ could be due in principle to the difference in the width of the Landau levels, but the anomalies in the behavior of the oscillation amplitudes in the phase-discontinuity region make it difficult to determine the width parameters in $Hg_{1-x}Cd_xTe$. However, the results obtained can also be understood by invoking another mechanism—the disruption of the oscillation periodicity due to effects related to the influence of terms linear in **k** in the Hamiltonian, which lead to lifting of the $H = 0$ degeneracy of the bands in the low-symmetry surface region.[11] In $Hg_{1-x}Cd_xTe$ this effect could be much more important than in InAs, due to the larger spin-orbit coupling of the former.

We should mention still another peculiarity in connection with oscillations in weakly-doped InAs. Whereas in the other samples the oscillations connected with the ground-state subband are well resolved both up to and beyond the onset of the first excited subband, in sample 1 the ground-state oscillations appear as a modulation on the significantly more distinct oscillations of the first excited subband for the entire range of voltages. The cause of such behavior will be considered later when we discuss the scattering mechanisms.

In Fig. 3 we present the surface carrier densities n_i in the subbands (i is the subband index) determined from the periods of the oscillations versus inverse magnetic field, as a function of $N_s = e^{-1}C_{ox}(V - V_0 - \varphi_s)$, where C_{ox} is the capacitance per unit area of the oxide, φ_s is the surface band bending, V_0 is the cutoff voltage of the function $n_0(V)$. We note that for a degenerate semiconductor the surface density N_s determined in this way does not equal the surface density of induced carriers (see below). For all samples a distinct threshold value $n_i = n_t = (9\pi/8)^{1/3}n^{2/3}$, was observed, reflecting the fact that in degenerate semiconductors the Fermi energy in the $2D$ subbands cannot be smaller than its bulk value.[6]

A characteristic feature of surface layers in InAs as compared to $Hg_{1-x}Cd_xTe$ is the persistence of magneto-oscillations in the capacitance associated with the first excited subband for N_s smaller than the onset values N_{s1} determined by extrapolating the function $n_1(N_s)$ to $n_1 = n_t$ (shown by the arrows in Fig. 3); at the edge of this region $n_1 \approx n_t$. In our view, such behavior could be caused by fluctuations in the surface potential, causing isolated regions of the surface layer in which the binding energy of the first

TABLE I.

Sample number	$n\times10^{-17}$ cm^{-3}	$\mu_H \times10^{-3}$ cm^2/V-sec	Γ_b, meV	E_{Fb}, meV	$n_t \times10^{-12}$, cm^{-3}	i	dn_i/dn_s Exper.	dn_i/dn_s Theor.	$n_s\times10^{-12}$ cm^{-2} Exp.	$n_s\times10^{-12}$ cm^{-2} Theor.	$m_{ci}/m_0\times10^3$ for $n_i=10^{12}$ cm^{-2} Exp.	$m_{ci}/m_0\times10^3$ for $n_i=10^{12}$ cm^{-2} Theor.	$m_{ci}/m_0\times10^3$ for $n_s=2\times10^{12}$ cm^{-2} Exp.	$m_{ci}/m_0\times10^3$ for $n_s=2\times10^{12}$ cm^{-2} Theor.	Δ,
1	0.23	52	3.0	12	0.12	0	0.705	0.641	0	0	45	36.5	46	39.0	—
						1	0.220	0.225	0.43	0.40	45	40	33	32.5	2
						2	0.070	0.080	1.53	1.51	—	41,5	26	26.7	2
						3	—	0.029	—	5.01	—	42,5	—	—	—
2	1.8	22	4.4	44	0.48	0	0.695	0.700	0	0	43	36.0	45	41.5	—
						1	0.230	0.230	0.80	0.85	44	38.5	34	32.5	2
						2	0.060	0.070	2.72	2.55	—	40	—	26.7	—
3	16	12	10.0	156	2.1	0	0.77	0.78	0	0	52	51,5	56	56	4
						1	0.23	0.22	2.9	2.3	55	55	44	44	4

Note: for sample 3, the value of m_{ci} is given for $n_s, n_i = 3\times10^{12}$ cm^{-2}.

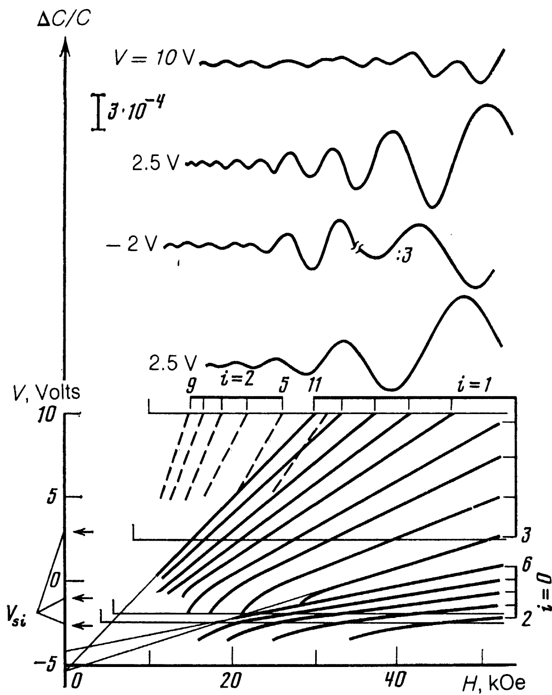

FIG. 2. Capacitance magneto-oscillations and positions of the oscillation maxima in a magnetic field for sample 2 as a function of voltage on the field electrode.

excited state is different from zero to persist even when $N_s < N_{s1}$. We note that for the ground-state subband such "seas" should be observed over a significantly smaller interval $N_s < N_{s0}$, in view of the significantly stronger dependence of the binding energy of this subband on φ_s (magneto-oscillations for $N_s < N_{s0}$ are observed experimentally for arbitrary orientations of the magnetic field, and are due to another effect—magneto-oscillations in the screening length[6]). As for the $i = 2$ subband, for which the influence of fluctuations is most effective, the magneto-oscillations near N_{s2} related to this subband are poorly resolved experimentally.

Turning now to the question of determining the total excess surface charge en_s, we note that this problem involves determination of the voltage which must be applied to the structure so that $n_s = 0$. In view of the high-frequency CVC, it would seem that this voltage can be determined from the flat-band capacitance C_{fb}; since within the depletion region and near the flat-band voltage V_{fb} the electron gas in the SCR is not quantized, C_{fb} can be calculated classically. Then the onset of the ground-state subband should be observed for $V = V_{s0} > V_{fb}$. However, for all the structures observed experimentally, the ground-state subband begins to fill for V significantly smaller than V_{fb}. This contradiction is due to the fact that in polar semiconductors there is a "deficit" of free carriers near the potential barrier at the junction interface, which leads to surface band bending and the formation of bound surface states even in the absence of an electric field, i.e., for $n_s = 0$.[12,13] The depth of the potential well φ_s for $n_s = 0$, as was shown in Ref. 13, can be determined from the relation

$$\frac{2a}{1+e\varphi_s/E_{Fb}}+\left(\frac{a}{1+e\varphi_s/E_{Fb}}\right)^{1/2}=\frac{e\varphi_s}{E_{Fb}},\qquad a=\frac{16}{9\pi a_B k_{Fb}},\qquad (1)$$

where E_{Fb} is the Fermi energy, a_B is the Bohr radius and k_{Fb} is the Fermi wave vector. Effects due to bulk free carriers are strikingly evident in sample 3, for which $F_{fb} \approx 155$ meV, while the value of φ_s determined from (1) is 55 meV. For a classical well, this value corresponds to an excess of surface carriers $n_s \approx 0.8 \times 10^{12}$ cm^{-2}. On the other hand, according to classical calculations (see section 5), the surface band bending needed to create the first excited bound state in this sample is ~ 62 meV, which is close to the $n_s = 0$ value of the band bending (this coincidence occurs also in samples 1 and 2). Thus, we can assume with reasonable accuracy that the condition $n_s = 0$ corresponds to the voltage for the onset of the ground-state subband, and n_s is given by the relation $n_s = C_{ox}(V - V_{s0} - \varphi_s)/e = N_s - C_{ox}(V_{s0} - V_0)/e$.

It is clear from the dependence of $n_\Sigma = \Sigma n_i$ on n_s shown in Fig. 4 that for all n_s the charge in the two-dimensional subbands is larger than the induced excess charge;

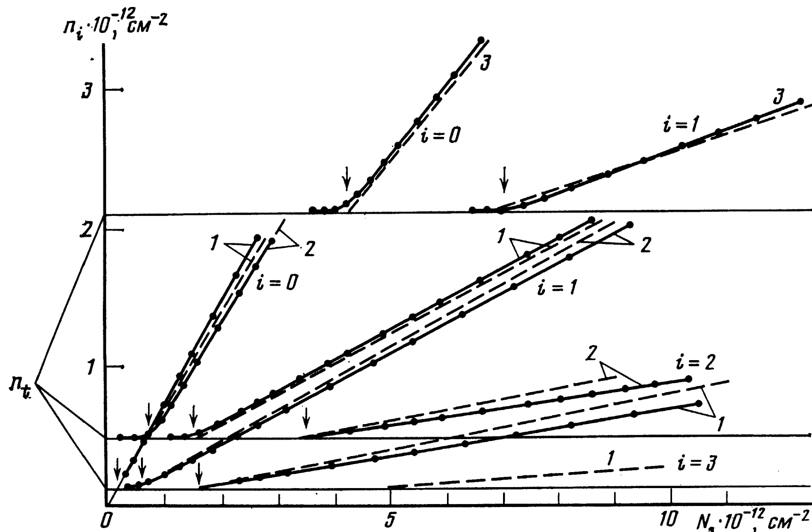

FIG. 3. Subband occupations as a function of $N_s = e^{-1}C_{ox}(V - V_o - \varphi_s)$. The numbers next to each curve denote the sample number. The continuous curves are experiment, the broken ones theory.

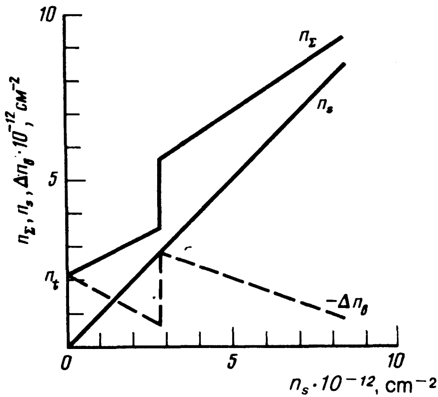

FIG. 4. Surface density of two-dimensional carriers n_Σ and the surface deficit of continuum electrons $-\Delta n_b$ for sample 3 as a function of surface density of induced carriers.

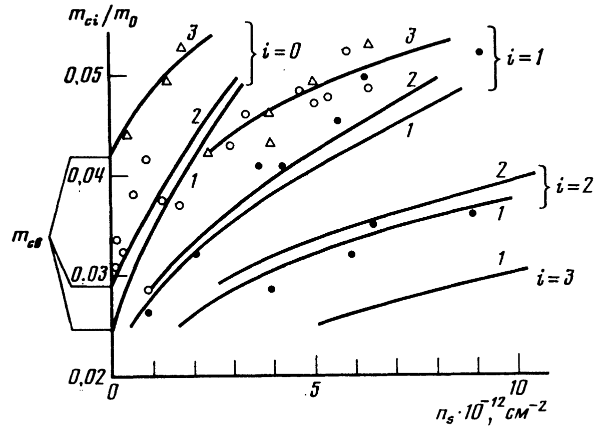

FIG. 5. The functions $m_{ci}(n_s)$. Continuous curves are calculations; the numbers next to each curve indicate sample numbers, the points are experiment: ●—sample 1, ○—sample 2, △—sample 3.

over a wide range of n_s, the quantity $\Delta n_b = n_s - n_\Sigma$ is comparable to n_s, As n_s increases, this difference decreases, i.e., the surface continuum-carrier deficit Δn_b decreases. At the population threshold of the next subband, Δn_b increases discontinuously to the value n_t, which corresponds to the transfer of a portion of the continuum electrons into the new bound state which, as we showed above, for a degenerate semiconductor fills discontinuously from $n_i = 0$ to $n_i = n_t$. We note that on the basis of Fig. 4 one would expect a population threshold for the next subband at $n_s \approx 10^{13}$ cm^{-2} (close to the value predicted by theory). Unfortunately, this value of n_s is close to the limit of experimental resolution in the structures under investigation.

The self-consistent variation of n_Σ and Δn_b ensures continuous CVC in the accumulation region. In the absence of this cancellation of the variations of n_Σ and Δn_b at the subband population thresholds, the functions $C(V)$ and dC/dV would exhibit discontinuities, which are not observed experimentally. In connection with this, it should also be noted that the classical calculation of the CVC leads to better agreement with experiment than calculations which take quantization in the SCR into account, while ignoring the influence of the continuum electrons.

4. BINDING ENERGIES AND DISPERSION-LAW

Parameters in the subbands

So as to determine the energy spectrum of electrons in accumulation layers (note that in the case of InAs, due to the nonparabolicity of the conduction band, the parameters of the spectrum depend on the surface band bending), along with the occupations n_i of the subbands we also determined the cyclotron masses m_{ci} of carriers in the subbands. Toward this goal, we studied the temperature dependences of the amplitudes of the capacitance oscillations in the space-charge region

$$\delta C_s \sim x(\operatorname{sh} x)^{-1}\exp(-xT_D/T), \qquad (2)$$

where $x = 2\pi^2 kT/\hbar\omega_{ci}$, T_D is the Debye temperature, and $\omega_{ci} = eH/m_{ci}c$ is the cyclotron frequency. The capacity of the MIS structure $C = C_{ox}C_s/(C_{ox} + C_s)$, which is nonlinearly related to C_s, is another experimentally measurable quantity. However, since the oscillation amplitude δC in the magnetic field is less than 0.01% of the value of C for $H = 0$, we have $\Delta C/C \approx (C/C_s)(\delta C_s/C_s)$ and when C/C_s is independent of temperature (which is easy to check experimentally), we can find m_{ci} by extracting the temperature dependence of the oscillation amplitudes from the directly-measurable capacitance of the MIS structure.

In the temperature interval $T = 1.8$ K to 30 K that we studied, and in magnetic fields up to 60 kOe, the m_{ci} determined from (2) increased somewhat (by 10–15%) as T and H increased, although the Dingle temperature and oscillations period did not depend on T or H within the limits of error. The cyclotron masses in the two-dimensional subbands, averaged over the different Landau levels and temperature intervals, are presented in Fig. 5 as functions of the surface excess charge n_s. In the two-band Kane approximation for the dispersion law in the subbands (this assumption agrees with the quasiclassical calculation described in the next section) the experimental quantities $n_{si} = k_{Fi}{}^2/2\pi$ (k_{Fi} is the two-dimensional Fermi quasimomentum in the ith subband) and m_{ci} are related to the dispersion-law parameters E_{gi} and m_{ni} by the functions

$$\frac{\hbar^2 k_{Fi}{}^2}{2m_{ni}} = (E_F - E_i)\left(1 + \frac{E_F - E_i}{E_{gi}}\right),$$

$$m_{ci} = m_{ni}\left(1 + 2\frac{E_F - E_i}{E_{gi}}\right), \qquad (3)$$

where $E_F - E_i$ is the chemical potential in the ith subband (in energy units). With the additional assumption that the matrix element P of the momentum operator between the Γ_6 and Γ_8 bands, which is related to the parameters E_{gi} and m_{ni} ($E_{gi}/m_{ni} = 4P^2/3\hbar^2$), has the same value as in bulk samples, we can determine from (3) the binding energies $|E_F - E_i - E_{Fb}|$ (E_{Fb} is the bulk chemical potential) and the parameters E_{gi} and m_{ni}. Corresponding results for sample 1 are shown in Fig. 6 (E_{gi} and m_{ni} are given in units of the corresponding bulk parameters). The subband binding energies for all ranges of n_s are noticeably smaller (particularly

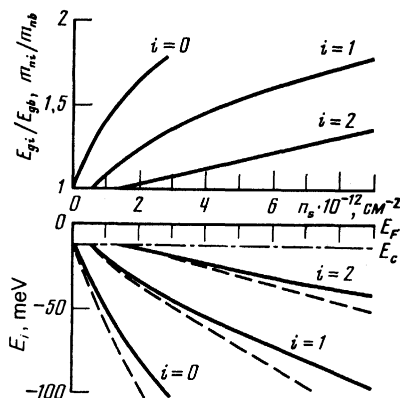

FIG. 6. Positions of the bottoms of the $2D$ subbands and dispersion-law parameters in the subbands as functions of n_s for sample 1. Continuous curves— from analysis of experimental data; broken curves—quasiclassical calculations.

for the ground state) than those determined in Ref. 4 from magneto-oscillations in the mobility due to the field effect $d\sigma/dV$ for materials with similar concentrations. This disagreement is due in part to the difference between the experimental values m_{ci} of the present work and the values used in Ref. 4, determined for material with a significantly lower concentration $n_b = 2\times10^{15}$ cm^{-3} from magneto-optic measurements. The basic cause of the difference, however, is connected with the fact that in Ref. 4 it was assumed in the analysis that the parameters E_{gi} and m_{ni} equalled their values in the bulk. However, in light of the results presented here (Fig. 6), as well as the results of available self-consistent calculations[14] (for other narrow-gap materials) such an assumption may not be justified.

The results for sample 2 can also be compared with the optical intersubband transition energies obtained in Ref. 8. At first glance, these energies agree better with the data in Ref. 4, i.e., they are close to the intersubband energies $E_i - E_j$ obtained in the present paper. However, for a degenerate electron gas the optical transitions are resolved only for those values of k_s for which the energy in the band of final states is larger than the Fermi energy, i.e., they occur in a region of rather large k_s. However, since the dispersion laws in the various subbands for a given n_s are different, and

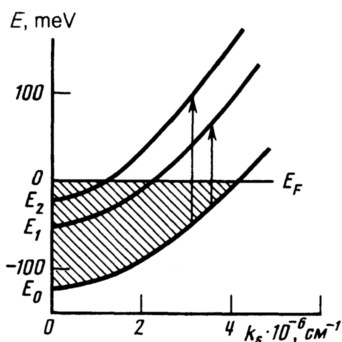

FIG. 7. Dispersion laws for $2D$ subbands in sample 1 for $n_s = 4\times10^{12}$ cm^{-2}, and intersubband transition energies from Ref. 8 (shown by arrows).

the intersubband spacings $E_i(k_s) - E_j(k_s)$ are functions of k_s (specifically, they increase with k_s), the energies of the intersubband transitions must be larger than the energy spacings $E_i - E_j$ between subbands for $k_s = 0$.

In Fig. 7 we show the functions $E_i(k_s)$ for the first three subbands in sample 2 for a surface density $n_s = 4\times10^{12}$ cm^{-2} corresponding to the conditions of the experiment in Ref. 8, calculated using (3) and the experimental values of E_{gi} and m_{ni}. On that figure we point out the transition energies $0\to1$ and $0\to2$ determined in Ref. 8. In our opinion, the agreement can be considered satisfactory.

5. COMPARISON WITH THEORY

Self-consistent calculations of the subband energy structure in InAs accumulation layers which take into account *ab initio* the nonparabolicity of the dispersion law are unknown to us. Calculations based on the simplest model, i.e., a linear potential which does not include screening, are less than satisfactory in their agreement with experiment (particularly for the excited bands). In view of the smallness of the effective mass and large value of $\varkappa$ in InAs, which lead to filling of several two-dimensional subbands and to comparatively large values of the average distance of the electrons from the surface, it is our opinion that one can expect an adequate description (at least for large n_s) of the electronic spectrum in the SCR within the framework of the quasiclassical approximation. In this case, for a given k_s the electronic energy in the ith subband $E_i(k_s)$ as measured from the bottom of the conduction band for $z=0$ can be found from the quasiclassical quantization of the electron motion in the direction perpendicular to the surface:

$$\int_0^{z_i} k_z\,dz = \int_{\mu_s}^{\mu_i} k_z(\mu)\left(\frac{d\mu}{dz}\right)^{-1} d\mu = \pi\left(i+\frac{3}{4}\right), \quad (4)$$

where $k_z(\mu)$ in the Kane two-band approximation is given by the relation

$$\frac{\hbar^2(k_s^2+k_z^2)}{2m_nE_g} = [\mu-\mu_s+\varepsilon_i(k_s)] + [\mu-\mu_s+\varepsilon_i(k_s)]^2. \quad (5)$$

Here $\mu(z)$ is the chemical potential normalized to E_g, $\mu_s = \mu(0)$, $\mu_b = \mu(\infty)$, $\varepsilon_i(k_s) = E_i(k_s)/E_g$, while the value of the chemical potential μ_i for the classical turning point z_i is found from equation (5) for $k_z = 0$. Screening is included in the calculation within the classical approximation, i.e., $d\mu/dz$ for a given μ_s is determined from the Poisson equation for the classical SCR. Non-parabolicity is taken into account within the two-band approximation, and the degeneracy in the bulk and SCR are assumed to be arbitrary. In the limiting case $T=0$ for a degenerate n-type semiconductor ($\mu_b \geqslant 0$) determination of the energy spectrum of the accumulation layer reduces to solving the equations[1]

$$\left(\frac{3\pi}{16}\right)^{1/2} \varepsilon_g^{1/4} \int_{\mu_i}^{\mu_s} \left\{\left[(\mu-\mu_s+\varepsilon_i)+(\mu-\mu_s+\varepsilon_i)^2 - \frac{\hbar^2 k_{si}^2}{2m_nE_g}\right]\right.$$
$$\times [(\mu_b-\mu)[\mu_b(1+\mu_b)]^{3/2}$$
$$\left. + \int_{\mu_b}^{\mu} [\mu(1+\mu)]^{3/2} d\mu]^{-1}\right\}^{1/2} d\mu = \pi\left(i+\frac{3}{4}\right), \quad (6)$$

where $\varepsilon_g = 2E_g \hbar^2 \varkappa^2 / m_n e^4$ is the width of the gap in units of the Bohr energy; $\varkappa = 14.9$ is the dielectric susceptibility of InAs.

In Figs. 3, 5, 6 we present the results of numerical calculations along with the experimental data. The calculated value of the filling rate dn_i/dn_s and threshold concentrations n_{si} are found to be in good agreement with their experimental values. In complete agreement with experiment, the theory predicts a strong dependence of n_{si} on the doping of the material, whereas dn_i/dn_s for identical numbers of subbands is practically independent of n_b (this is also true in inversion layers). For the same values of ε_g and for a wide range of narrow-gap semiconductors the $\varepsilon_g^{1/4}$ variation is actually insignificant, and for similar doping levels (similar μ_b) theory predicts that the occupation parameters and intersubband energies depend weakly on the width of the gap E_g. This is also in good agreement with experiment. A comparison of the data for sample 1 of the present work with occupation parameters investigated earlier for accumulation layers of $Hg_{1-x}Cd_xTe$ of various compositions will serve as an illustration of this (see samples 2, 8 of Ref. 6).

The calculated values of the cyclotron masses and binding energies are in somewhat worse agreement with experiment; notably the theory somewhat underestimates m_{ci} and correspondingly overestimates $E_c - E_i$. However, here also the difference for samples 1 and 2 are less than 15%, while for sample 3 theory and experiment agree within the limits of error. As calculations show, the dispersion laws $E_i(k_{si})$, as we assumed in the last section, can be approximated to high accuracy by expression (3). However, the dependence of the parameters E_{gi} and m_{ni} on n_s is weaker than that which follows from analysis of the experimental data.

The results we have presented, in our opinion, attest to the applicability of the quasiclassical approximation in calculating the electronic spectrum in surface layers of narrow-gap semiconductors. However, it must be noted that since these calculations are not self-consistent, the total surface carrier density in the quantized surface potential well will differ somewhat from the value n_s obtained for a classical well of the same depth.

6. SCATTERING MECHANISMS

The SCR differential capacitance is determined only by the density of states, and (as opposed to the surface channel conductivity) does not depend on the mobility. However, since scattering is reflected to a considerable degree in features of the density of states in the presence of a quantizing magnetic field (it determines the width of the Landau levels), investigations of capacitance magneto-oscillations, notably the field dependence of the oscillation amplitudes, also allow us to obtain information on the scattering mechanisms.

For all the subbands and all samples, the dependence of the oscillation amplitude δC on magnetic field is satisfactorily linearized in the coordinates $\ln(\delta C \operatorname{sh} x/x) - x$, which, consistent with (2), allows us to infer that the width of the levels $\Gamma = \pi k T_D$ is independent of the Landau level index. In the temperature interval 1.8 K to 30 K (within which limits it is possible to analyze the oscillation amplitudes) Γ is also independent of temperature.

When scattering by ionized donors with a surface density $N_{di} = n_b z_i$ (z_i is the effective weighted average in the z-direction for the ith subbands) is taken into account, along with scattering by the built-in oxide charge eN_{ox} and by surface roughness, the width of levels in the ith subband $\Gamma_i = \Gamma_{di} + \Gamma_{oxi} + \Gamma_{ri}$, where the partial broadening, without including the effects of intersubband screening, can be written in the form[16,17]

$$\Gamma_{di} = \frac{\pi}{16}\varepsilon_{bi}\frac{N_{di}}{n_i}, \qquad \Gamma_{oxi} = \frac{\pi}{16}\varepsilon_{bi}\frac{N_{ox}}{n_i},$$
$$\Gamma_{ri} = 8\pi^3 \varepsilon_{bi} (n_s L\Delta)^2 \Phi\left(\frac{3}{2}, 2, -\beta\right), \tag{7}$$

where $\varepsilon_{bi} = m_{ci} e^4 / 2\hbar^2 \bar{\varkappa}^2$ is the effective Rydberg for the ith subband, $\bar{\varkappa} = (\varkappa + \varkappa_{ox})/2; \varkappa_{ox} = 10$ is the dielectric permittivity of the oxide,[18] L, Δ are roughness parameters, and $\Phi(3/2, 2, -\beta)$ is a confluent hypergeometric function with $\beta = k_{Fi}^2 L^2$. We note that corresponding to the results presented in section 5, the concentration dependences of the level widths (especially since the mobilities satisfy $\mu_i \sim (m_{ci})^2$) to a significant extent are determined by the increase of $\varepsilon_{bi} \sim m_{ci}$ as $n_s(n_i)$ increases.

As is clear from the functions $\Gamma_i(n_s)$ presented in Fig. 8, for subbands with the same index (at least near the subband population thresholds), Γ_i increases significantly with increasing doping; this fact attests to the important, and in samples 2, 3 dominant, contribution of scattering by ionized donors, and is related both to the high level of doping and to the relatively larger values of z_i in narrow-band semiconduc-

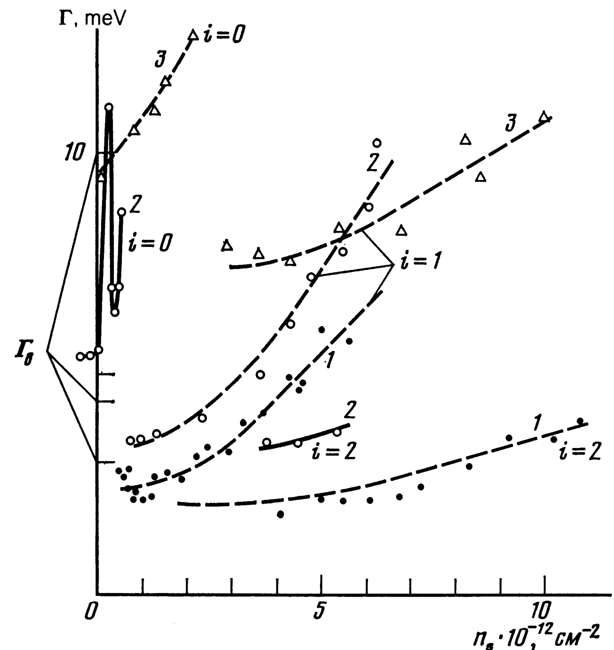

FIG. 8. Width of Landau levels in $2D$ subbands as a function of n_s. The numbers next to the curves are sample numbers; the points are experiments: ●—sample 1; ○—sample 2, △—sample 3. The broken curves are calculations.

tors. Near the ground subband population threshhold, a rough approximation to N_{d0} can be estimated as $n_b z_0 \approx n_1$, and since many-band effects in this case can be neglected, $\Gamma_{d0} \approx \pi\varepsilon_{b0}/16$, which to within a logarithmic factor coincides with the corresponding value for scattering by ionized impurities in bulk samples $\Gamma_b = (2/3\pi)\varepsilon_b(N_d/n) = (2\varepsilon_b/3\pi)$. This correspondence is confirmed experimentally. The widths Γ_b determined from the Shubnikov–de Haas oscillations correlate satisfactorily with the values $\Gamma_{d0} \approx \Gamma_0 - \Gamma_{ox0}$ where Γ_{ox0} is calculated starting with the flat-band charge (the contribution of roughness near onset, as will be shown below, can be neglected). We note that in sample 3, since $n_i \gg n_t > N_{ox}$, the contribution of scattering by the oxide charge for all n_s is at most 5–6% even for the ground-state subband, while in sample 2 for small n_0 it reaches 20%.

In the case of several filled subbands, analysis even in the framework of simple scattering models is complicated by the necessity of including the effects of screening by carriers of other subbands and of intersubband scattering processes. In the first approximation, since (as shown above) $n_i \gg n_{i+1}$ and $z_i < z_{i+1}$, the influence of higher-index subbands on the scattering in lower subbands can be neglected. For excited subbands, however, the carriers in the more populated subbands with smaller i effectively screen both the scattering potentials associated with the boundary and the potential of the ionized impurities.

Screening of the oxide charge in rough approximation can be included by introducing a factor n_i/n_s in the expression for $\Gamma_{oxi} \to \Gamma_{oxi} n_i/n_s$. As for screening of the charged donors, here it is necessary to include the details of the electron density distribution in the excited subbands throughout the accumulation layer, related to the presence of nodes of the wave functions which describe the motion of an electron in the direction perpendicular to the surface. Actually, screening of charged donors by carriers in other subbands is effective only for those carriers in the excited subbands which are distributed spatially in the same region as that of the carriers of the lower subbands. As estimates based on the quasiclassical approach investigated above show, the extent of the ith subband $z_i \approx (i+1)z_0$ (z_0 is the extent of the ground-state subband), i.e., in the first excited subband approximately half the electrons are spatially distributed in the same region as the ground-state subband carriers, in the second excited subband $\sim 1/3$, etc. In this case, the broadening due to donor scattering, taking screening into account, can be approximately described by the form $\Gamma_{di} \approx \Gamma_b(1 + n_i/n_{i-1})/(i+1)$. Using the relations presented above to calculate the width $\Gamma_i = \Gamma_{di} + \Gamma_{oxi}$ of levels near the population thresholds of the subbands, and the experimental data given above for the subband populations and cyclotron masses, we obtain, e.g., for sample 1 the values $\Gamma_1 = 2.35$ meV, $\Gamma_2 = 2.0$ meV. As is clear from Fig. 8, such estimates are found to be in good agreement with the experimental values of Γ_i (this also obtains for other samples) and explain the observed increase in width of the levels near the subband population thresholds as the subband index increases.

The increase in Γ_i with increasing n_s observed experimentally for all subbands is related to scattering by surface roughness. Here, because the surface electric field $E_s = 0$ near the population threshold of the ground-state subband (i.e., for $n_0 \approx n_t$), as shown in section 3, in expression (7) for $\Gamma_{r0} \sim (n_s L\Delta)^2$ we should use $(n_0 - n_t)$ in place of n_s. For the excited subbands it is also necessary to take into account screening of the potential fluctuations due to surface roughness, which are distributed spatially close to the boundary, by carriers in the lower subbands which (it is not difficult to show) leads to the approximate expression

$$\Gamma_{ri} = 8\pi^2\varepsilon[(n_i - n_t)L\Delta]^2\Phi(^3/_2, 2, -\beta),$$

where $\beta = 2\pi n_i L^2$. The noticeable decrease of $d\Gamma_i/dn_s$ at constant n_s as the index number i of the subband increases points to the necessity of such considerations. The dashed lines in Fig. 8 show the results of calculating $\Gamma_i = \Gamma_i^0 + \Gamma_{ri}$ where Γ_i^0 is the width due to scattering by ionized donors and oxide charges, and varies only weakly as n_s increases (in the calculations, Γ_i^0 was taken to be constant and equal to the value of Γ_i determined near the subband population threshhold). The average displacement Δ and correlation length L which were used in these calculations and which were determined from the best fit to experiment, are presented in the table. The similarity of the parameters Δ and L from one subband to another in the same sample can be regarded as an argument in favor of the correctness of the approximations used.

The results which relate to the ground-state subband of sample 2 require special discussion. From the dependences of the level widths on V shown in Fig. 9, it is apparent that Γ_0 exhibits a sharp peak in a narrow bias region near the population threshold of the first excited subband; in the neighborhood of the maximum, Γ_0 increases by almost a factor of two. Such behavior is characteristic of all the structures made on sample 2 that we investigated, and attests to the switching-on of an additional relaxation channel in a narrow range of variation of the surface band-bending; this new

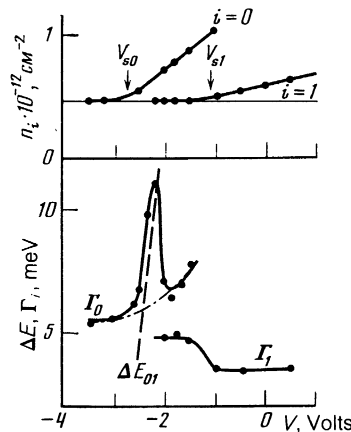

FIG. 9. Subband occupations, level widths and intersubband energies $\Delta E_{01} = E_1 - E_0$ (broken curve) for sample 2 (near the population threshold of the first excited subband).

channel is most naturally related to intersubband scattering. The effectiveness of intersubband scattering depends significantly on the energy spacing between subbands, and it is of interest to compare data on the broadening with the subband energy structure. On the same figure, the dashed line shows the energy difference $\Delta E_{01} = E_0 - E_1$ of the bottoms of the subbands, calculated on the basis of the experimental values n_0 and n_1. As is clear from the figure, the position of the peak Γ_0 occurs just in the concentration region where ΔE_{01} is on the order of the level linewidths, which is also to be expected from the mechanism we have discussed. It is necessary to note that the existence of a range of band bendings in which $\Delta E_{01} \sim \Gamma$ is related to a significant extent to the presence of pinning of n_1 in the region $V < V_{s1}$. In light of the results presented here, we find an explanation for the poorly-resolved oscillations due to carriers in the ground-state subband of sample 1. The population thresholds of the first two excited subbands in this sample are separated by an interval smaller than N_s (Fig. 3), while the "tail" dependence $n_1(N_s)$ extends up to n_{s0}, in connection with which even the intersubband scattering is quite close to the population threshold of the ground-state subband.

In view of the detailed nature of the spatial distribution of carriers in the excited subbands, one should expect less influence of the intersubband scattering on the level width of the first excited subband. Actually, as we showed above, Γ_1 is determined primarily by those carriers which are spatially separated from the region where the ground-state subband carriers are localized. However, since intersubband scattering of electrons is absent in this region, variation of Γ_1 because of intersubband scattering is smaller than variation of Γ_0. The experimentally-observed increase in Γ_1 for sample 2 in the pinning region (Fig. 9) may, generally speaking, have another explanation: if the oscillations in the first excited subband for $V < V_{s1}$ are related to the creation of "seas" for carriers in this subband (because of rather long-period fluctuations in φ_s), then for not-too-large n_t the broadening can be related to a diversity of n_1, and possibly even n_t, in the various "seas."

The results we have presented show that although carriers in the ground-state subband constitute about 2/3 of the overall surface density n_s, the contribution of excited subbands to the total conductivity of the channel cannot be ignored. Furthermore, because of the smaller values of effective masses and the screening effects connected with them, the partial conductivity $\sigma_i = en_i\mu_i$ can be larger than the conductivity of the ground-state subband. Ignoring this circumstance in analyzing experimental data obtained, e.g., from measurements of the effective mobility or the field-effect mobility, can lead to incorrect conclusions relative to the scattering parameters. What we have said here applies equally well to inversion layers based on narrow-gap semiconductors.

(1) We will not dwell on details of the calculation, since prior to the submission of this article there appeared in print a paper by Ando,[15] in which the $2D$ subband spectrum in InSb was calculated using the quasi-classical approximation for the case $T = 0, \mu_b = 0$. For $\mu_b = 0$, equation (6) leads to the relation (2.11) of Ref. 15.

[1]D. C. Tsui, Phys. Rev. **B8**, 2657 (1973).
[2]G. M. Min'kov and V. V. Kruzhaev, Fiz. Tverd, Tela (Leningrad) **22**, 1641 (1980) [Sov. Phys. Solid State **22**, 959 (1980)].
[3]E. Yamaguchi, Phys. Rev. **B32**, 5280 (1985).
[4]H. Reisinger, H. Shaber, and R. E. Doezema, Phys. Rev. **B24**, 5960 (1982).
[5]H. A. Washburn, J. R. Sites, and H. H. Wieder, J. Appl. Phys. **50**, 4872 (1979).
[6]T. I. Deryabina, V. F. Radantsev, L. P. Zverev *et al.*, Zh. Eksp. Teor. Fiz. **88**, 2088 (1985) [Sov. Phys. JETP 61, 1234 (1985)].
[7]T. I. Deryabina, L. P. Zverev, and V. F. Radantsev, Fiz. Tekh. Poluprovodn, **17**, 2065 (1983) [Sov. Phys. Semicond. **17**, 1319 (1983)].
[8]H. Reisinger and F. Koch, Solid State Commun. **37**, 429 (1981).
[9]W. Zhao, F. Kock, J. Ziegler, and H. Maier, Phys. Rev. **B31**, 2416 (1985).
[10]V. M. Bazovkin, G. L. Kurushev, and V. G. Polovinkin, Phys. Status Solidi **A74**, 297 (1982).
[11]Yu. A. Bychkov and E. I. Rashba, J. Phys. **C17**, 6039 (1984).
[12]O. V. Konstantinov and A. Ya. Shik, Zh. Eksp. Teor. Fiz. **58**, 1662 (1970) [Sov. Phys. JETP **31**, 891 (1970)].
[13]G. A. Baraff and J. A. Appelbaum, Phys. Rev. **B5**, 475 (1972).
[14]T. Takada, K. Arai, and Y. Uemura, *Lecture Notes in Physics* **152**, 101 (1982).
[15]T. Ando, J. Phys. Soc. Jpn. **54**, 2676 (1985).
[16]S. M. Goodnick and D. K. Ferry, Thin Solid Films **103**, 27 (1982).
[17]T. Ando, A. B. Fowler, and F. Stern, Rev. Mod. Phys. **54**, 563 (1982).
[18]D. A. Baglee, D. K. Ferry, and C. W. Wilmsen, J. Vac. Sci. Technol. **17**, 1032 (1980).

Translated by F. J. Crowne